

IPACK2007-33993

LOOP THERMOSYPHON DESIGN FOR COOLING OF LARGE AREA, HIGH HEAT FLUX SOURCES

**John R. Hartenstine, Richard W. Bonner III,
Jared R. Montgomery**
Advanced Cooling Technologies, Inc.
1046 New Holland Avenue
Lancaster, PA 17601
Phone: (717)295-6112, Fax: (717)295-6064
John.Hartenstine@1-act.com

Tadej Semenic
University of California, Los Angeles
Department of Mechanical Engineering
420 Westwood Plaza
Los Angeles, CA 90095-1597
Phone: (310)825-8185, Fax: (310)206-4830

ABSTRACT

Two-phase flow loop technologies capable of acquiring high heat fluxes ($>1\text{kW}/\text{cm}^2$) from large area heat sources (10cm^2) are being considered for the next generation naval thermal requirements. A loop thermosyphon device (~ 1 meter tall) was fabricated and tested that included several copper porous wick structures in cylindrical evaporators. The first two were standard annular monoporous and biporous wick designs. The third wick consists of an annular evaporator wick and an integral secondary slab wick for improved liquid transport. In this configuration a circular array of cylindrical vapor vents are formed integral to the primary and secondary transport wick composite. Critical heat fluxes using these wick structures were measured between $240\text{W}/\text{cm}^2$ and $465\text{W}/\text{cm}^2$ over a 10cm^2 area with water as the working fluid at 70°C saturation temperature. A thermosyphon model capable of predicting flow rate at various operating conditions based on a separated flow model is presented.

INTRODUCTION

Future thermal management requirements for the Navy's warships will include advanced power electronics, advanced radar, dynamic armor and weapons systems. It is anticipated that shipboard cooling requirements will double every six years [1]. In the past 50 years, the volume of electronics enclosures have been reduced by 99%, while the power output has increased to $50\text{kW}/\text{ft}^3$, and switching frequencies are now greater than 20kHz . With advances in materials, packaging and switching rates, the heat fluxes are expected to reach $1\text{kW}/\text{cm}^2$. An evaluation of the heat load distribution on the All Electric

Ship found that the semiconductors accounted for over 70% of the total heat generated while occupying just over 5% of the volume. As a result there is a need for advanced cooling technologies that can transfer large waste heat loads at high heat fluxes ($1\text{kW}/\text{cm}^2$). A number of thermal management technologies have been identified as potential solutions for cooling the power electronics on the All Electric Ship, including advanced heat pipe designs utilizing advanced wick structures.

Advanced Cooling Technologies, Inc. (ACT), was subcontracted by the University of California, Los Angeles (UCLA) through the United States Navy, Office of Naval Research to (1) provide support for the fabrication of biporous copper samples for high heat flux testing by UCLA and (2) develop a two-phase flow loop technology utilizing a biporous wick structure capable of acquiring heat fluxes greater than $1\text{kW}/\text{cm}^2$ from a 10cm^2 heat source. The development and evaluation of the biporous wicks used in this study are described by Semenic et al. [2], [3] and Lin et al. [4]. The design requirements for the prototype two-phase cooling loop are as follows:

- Heat Flux: $1\text{kW}/\text{cm}^2$
- Heat Input Area: 10cm^2
- Total Heat Load: 10kW
- Maximum Junction Temperature: 125°C

In the design phase, ACT evaluated several two-phase technologies that would be potentially suited to incorporate

high heat flux wick structures and be practical for the Navy's shipboard applications. These technologies included loop heat pipes, vapor chambers (planar heat pipes), evaporative spray cooling loops and loop thermosyphons. The loop thermosyphon concept was selected for demonstration in this project because: (1) loop thermosyphons are inherently simple and reliable heat transport devices that are particularly suited for robust shipboard cooling requirements; (2) loop thermosyphons have been used in the past for heavy industrial applications such as waste heat recovery from process equipment; and (3) loop thermosyphons can have flexible transport lines for installation convenience.

Previous loop thermosyphons typically have a liquid pool in the evaporator and rely on flow and pool boiling directly on the tube wall for heat transfer. These boiling mechanisms without surface modification are less efficient (i.e. lower heat transfer coefficients, large ΔT 's to initiate nucleate boiling) and cannot handle high heat fluxes (i.e. low critical heat fluxes). ACT proposed an innovative loop thermosyphon design that includes a porous wick structure in the evaporator fed by the circulating two-phase flow of the thermosyphon, and partially by capillary forces developed at the vapor-liquid interface of the porous wick at low fluid charges.

NOMENCLATURE

C	Constant in two-phase multiplier
D	Local diameter of the pipe
f	Friction factor
f_{liq}	Liquid flowing alone friction factor
f_{vap}	Vapor flowing alone friction factor
g	Gravitational constant
G	Mass velocity
$L_{1\phi}$	Single phase length
$L_{2\phi}$	Two-phase length
L_{tot}	Total axial length of thermosyphon
m	Fluid mass
$P_{f,1\phi}$	Single phase frictional pressure drop
P_g	Gravitational pressure drop
$P_{f,liq}$	Two-phase frictional pressure drop term, defined as pressure drop of single phase liquid flowing alone in the tube
$P_{f,vap}$	Two-phase frictional pressure drop term, defined as pressure drop of single phase vapor flowing alone in the tube
$P_{f,tot}$	Actual two-phase frictional pressure drop

$P_{1\phi,tot}$	Total single phase pressure drop
$P_{2\phi,tot}$	Total two-phase pressure drop
Re	Reynolds number
Re_{liq}	Reynolds number with liquid flowing alone
Re_{vap}	Reynolds number with vapor flowing alone
V_{liquid}	Liquid velocity
V_{vap}	Vapor velocity
x	Vapor quality
XLM	Lockhart-Martinelli parameter
z	Axial position
α	Void fraction of liquid
ρ_{liq}	Liquid density
ρ_{vap}	Vapor Density
ϕ_{vap}	Two-phase vapor frictional pressure drop multiplier
μ_{liq}	Liquid viscosity
μ_{vap}	Vapor viscosity

LOOP THERMOSYPHON MODELING

The loop thermosyphon was designed to continually supply enough liquid water to meet the requirements of a $1\text{kW}/\text{cm}^2$ heat flux over a 10cm^2 surface area. A simplified schematic of a loop thermosyphon is shown in Figure 1, to better describe the modeling domain. The driving force for the passive loop thermosyphon design is in the head of liquid under the condenser. The head of liquid acts to displace the less dense vapor in the evaporator, creating a two-phase flow towards the condenser. It is noted that the current loop thermosyphon is approximately 1 meter in height. The total height is much higher than traditional heat pipes/thermosyphons. In cases with less gravitational head, fluid exits the pool as single-phase saturated vapor after phase change in the evaporator (and may be driven by the capillary forces of a wick). The added gravitational head in this study is sufficient to drive excess liquid flow to the evaporator generating two-phase flow towards the condenser. The presence of the wick structure on the tube wall does not aid in flow circulation (as there is no separation between single-phase liquid and single-phase vapor) and provides negligible frictional resistance to the flow, as the wick can be thought of as a thin walled surface modification. It is again noted that the wick will aid in the circulation of fluid in loop thermosyphons with less gravitational head where the returning liquid feeds a wick/wicked pool. The described model is for the case of flow boiling, with excess liquid provided to the evaporator.

The flow resistances of the loop include the frictional, gravitational, and acceleration pressure drops in the various channels of the loop [5]. The acceleration pressure drops are neglected for simplicity, as any acceleration of the evaporating liquid in the evaporator will be balanced by the de-acceleration of the condensing vapor in the condenser in this closed loop system. A computer program was written with the main goal of predicting the mass flow rate in the loop based on the operating conditions of the loop (condenser coolant temperature and evaporator power input). The program iterates the mass flow rate by attempting to maintain the pressure balance in the system, mainly the gravitational head of the condensing liquid equaling the gravitational head losses and frictional pressure drops in the rest of the system.

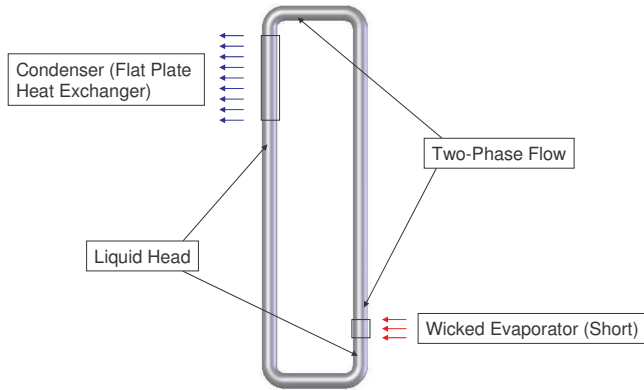


Figure 1. A simplified schematic of the loop thermosyphon is depicted to aid in the discussion of the loop thermosyphon model (see Figure 4 for a detailed solids model of the fabricated loop thermosyphon).

An oversized condenser/excess liquid reservoir and a relatively small evaporator allow some simplifying assumptions to be made to the model. In typical loop thermosyphon systems the heat input to the evaporator causes a gradient in vapor quality along the evaporator length. In the current case this vapor quality gradient could be neglected because the evaporator length was negligible (12.7mm) compared to the overall two-phase length (1m). In other words the evaporator pressure drop could be solved without integration over the evaporator length. The volume of the condenser was large compared to the overall system, so any excess fluid would build up in the bottom of the condenser/reservoir. The condenser/reservoir also has a large cross sectional area, so the excess liquid does not add any significant gravitational head. This allows the location of the two-phase/liquid head location to be accurately approximated at the bottom of the condenser. The equations used in this loop thermosyphon model are summarized in Equation 1 through Equation 21.

The mass charge in the liquid and two-phase section was calculated using Equation 1 for the mass charge based on the local void fraction of liquid in the loop. The calculation of the

mass gives a better approximation as to how much liquid needs to be present in the closed loop system. Excess liquid in the loop will lead to a larger thermal resistance on the condenser. Lower liquid heights caused by undercharging will lead to a lower flow rate of liquid to the evaporator.

$$m = \int_0^{L_{tot}} \frac{\pi D^2}{4} (\rho_{liq} (1 - \alpha) + \rho_{vap} \alpha) dz \quad (1)$$

The equations used to calculate the gravitational and frictional pressure drops in the single phase section of the loop are summarized in Equation 2 through Equation 8. Equation 2 describes the frictional pressure drop of the single phase liquid. Equation 3 and Equation 4 describe the friction factor models used for the laminar and turbulent flow transitions. The gravitational pressure drop (gain) was calculated using Equation 5 with the void fraction equal to zero as shown in Equation 6. The gravitational constant in the liquid line is equal to zero in the horizontal sections (Equation 7) and negative in the liquid line (Equation 8). The total pressure change is the integral of the pressure drop derivatives over the single phase length, as shown in Equation 9.

$$\frac{dP_{f,1\phi}}{dz} = -\frac{2f_{liq} G^2}{D\rho_{liq}} \quad (2)$$

$$Re < 2300, \quad (3)$$

$$f = \frac{64}{Re}$$

$$Re > 2300, \quad (4)$$

$$f = \frac{0.316}{Re^{1/4}}$$

$$\frac{dP_g}{dz} = -g(\rho_{vap} \alpha + \rho_{liq} (1 - \alpha)) \quad (5)$$

$$\alpha = 0 \quad (6)$$

$$g = 0 \quad (7)$$

$$g = -9.81 \quad (8)$$

$$\Delta P_{1\phi, total} = \int_0^{L_{1\phi}} \left(\frac{dP_{f,1\phi}}{dz} + \frac{dP_g}{dz} \right) dz \quad (9)$$

The equations used to calculate the gravitational and frictional pressure drops in the two-phase section of the loop are summarized in Equation 10 through Equation 21. Equation 5 is again used in the two-phase section, with the gravitational

constant positive (Equation 10) in the vertical sections and zero in the horizontal sections. The void fraction is evaluated using Equation 11, an empirical model based on the Lockhart-Martinelli parameter developed by Wallis [6]. The Lockhart-Martinelli parameter is defined in Equation 12 as the ratio of the pressure drop if the liquid flow rate were occupying the whole diameter to the pressure drop if the vapor flow rate was occupying the whole diameter [7, 8]. The pressure drops for the vapor and liquid flowing alone defined in Equation 13 and Equation 14 are calculated using the Reynolds numbers defined in Equation 16 and Equation 17. These Reynolds numbers are used with Equation 3 and Equation 4 to determine the appropriate friction factors. The actual two-phase frictional pressure drop (Equation 15) is then the pressure drop of the vapor flowing alone times a two-phase multiplier. The value of the two-phase multiplier is calculated using Equation 18, with the value of C dependent on the turbulence regime of the liquid and vapor described in Equation 19 and Equation 20. The total two-phase pressure drop due to friction and gravity is then the integrated over the entire two-phase length in Equation 21. Equation 22 shows the pressure balance maintained when the appropriate mass flow rate is converged upon.

$$g = 9.81 \quad (10)$$

$$\alpha = (1 + XLM^{0.8})^{-0.378} \quad (11)$$

$$XLM^2 = \frac{\frac{dP_{f,liq}}{dz}}{\frac{dP_{f,vap}}{dz}} \quad (12)$$

$$\frac{dP_{f,vap}}{dz} = \frac{2f_{vap}G^2x^2}{D\rho_{vap}} \quad (13)$$

$$\frac{dP_{f,liq}}{dz} = \frac{2f_{liq}G^2(1-x)^2}{D\rho_{liq}} \quad (14)$$

$$\frac{dP_{f,tot}}{dz} = \phi_{vap}^2 \frac{dP_{f,vap}}{dz} \quad (15)$$

$$Re_{vap} = \frac{\rho_{vap}V_{vap}D}{\mu_{vap}} \quad (16)$$

$$Re_{liq} = \frac{\rho_{liq}V_{liq}D}{\mu_{liq}} \quad (17)$$

$$\phi_{vap}^2 = 1 + C(XLM) + XLM^2 \quad (18)$$

$$Re_{vap} > 2300, \quad (19)$$

$$Re_{liq} < 2300, C = 5$$

$$Re_{liq} > 2300, C = 10$$

$$Re_{vap} < 2300, \quad (20)$$

$$Re_{liq} < 2300, C = 12$$

$$Re_{liq} > 2300, C = 20$$

$$\Delta P_{2\phi,total} = \int_0^{L_{2\phi}} \left(\frac{dP_{f,tot}}{dz} + \frac{dP_g}{dz} \right) dz \quad (21)$$

$$\Delta P_{2\phi,total} + \Delta P_{1\phi} = 0 \quad (22)$$

Using the model described above, the pressure drop and flow rate predictions for the loop were predicted for power inputs ranging from 0.25kW_{th} to 10kW_{th} at a loop operating temperature of 70°C. Figure 2 shows the pressure drops for each part of the loop. All pressure differences are defined as positive even though the vertical ΔP should be the opposite sign because this line increases due to gravity. To maintain the pressure balance described in Equation 22 the vertical liquid pressure drop minus the other three components should be equal to zero. The vertical liquid pressure drop slowly increases because the frictional pressure drop in the line decreases as the flow rate decreases. The decrease in flow rate versus power is shown in Figure 3. The decrease in flow rate after 1.5kW_{th} is due to the increase in two-phase ΔP because of the increase in vapor quality (at relatively constant void fraction). The flow rate increases below 1.5kW_{th} because the difference in gravitational head between the single and two-phase lengths is increasing faster than the increase in frictional pressure drop due to the rapid increase in void fraction at low thermal power. The vapor quality changes rather linearly with power as the flow rate is near constant. At 10kW_{th}, the vapor quality leaving the evaporator is 0.25, well below complete dryout conditions.

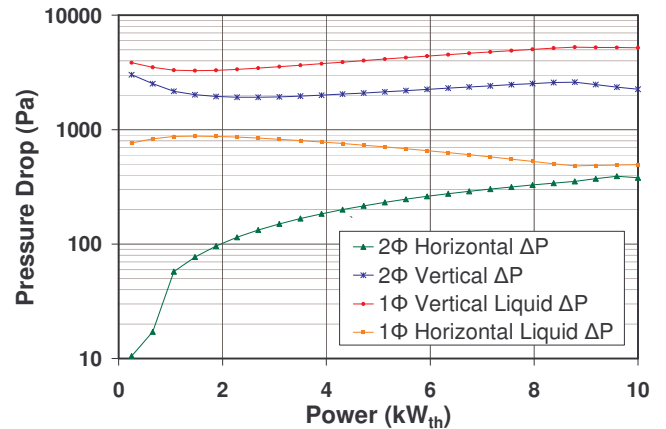


Figure 2. The predicted pressure drops for the various segments of the loop thermosiphon are depicted.

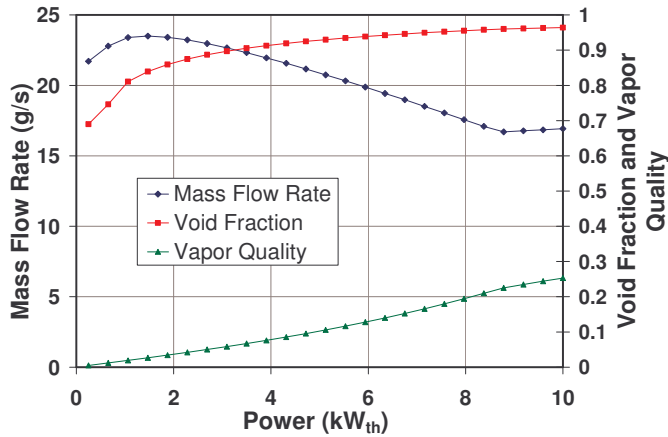


Figure 3. The predicted mass flow rate, void fraction, and vapor quality for the loop thermosyphon are plotted versus power.

EXPERIMENTAL APPARATUS

A schematic of the loop thermosyphon is shown in Figure 4. The critical elements of the loop thermosyphon assembly include the removable evaporator region, the vapor transport line, the condenser, and the liquid return line. The geometry of the final prototype design is documented in Table 1. The copper evaporator was 25.4mm diameter x 127mm long and was brazed to a cylindrical heater block to supply the required thermal loading for test. A length of tubing below the heat input to the evaporator was included to allow for flow development below the heat input region. The vapor transport line was 19.05mm diameter and extended approximately 1m above the evaporator. The condenser was a flat plate heat exchanger plumbed for counter current flow with cooling water. The flat plate heat exchanger was sized to accommodate 10kW_{th} with negligible pressure drop on the process fluid side. The liquid return line exiting the flat plate heat exchanger was 6.35mm diameter and extended to the bottom of the evaporator. A glass tube was attached within a section of the liquid return line for visual observation of the returning fluid flow. The glass tube was placed in line with the evaporator region to make notation of the liquid level easier at low fluid charging. With the exception of the glass region, both the vapor and liquid lines were manufactured from copper.

Three evaporator wick structures were fabricated and tested. The first two were standard copper monoporous and biporous designs, respectively. The annular construction of these two wicks covered the 127mm evaporator length and was 2mm thick. The third wick design was a copper biporous structure consisting of an annular configuration attached to the heat input surface wall and an integral secondary slab wick for improved liquid transport. A circular array of vapor vents was formed within the slab wick. The loop thermosyphon was designed so that each of the wick designs described above could be interchanged by replacing the evaporator region.

Photographs of an annular designs and the slab wick design with vapor vents are shown in Figure 5.

Table 1. Loop Thermosyphon Design Parameters.

Materials	
Evaporator/Transport Line Material	Copper
Evaporator Wick Material	Copper
Working Fluid	Water
Requirement	Parameter
Dimensions	
Evaporator Configuration	25.4mmOD x 12.7cm Long
Condenser Configuration	Flat Plate Design
Transport Distance Between Evaporator and Condenser	
Vapor Line Diameter	19.05mm x 0.89mm thick
Vapor Line Length, Vertical	1.0 m
Vapor Line Length, Horizontal	0.16m
Liquid Line Diameter	6.35mm
Liquid Line Length, Vertical	0.80 m
Liquid Line Length, Horizontal	0.16m

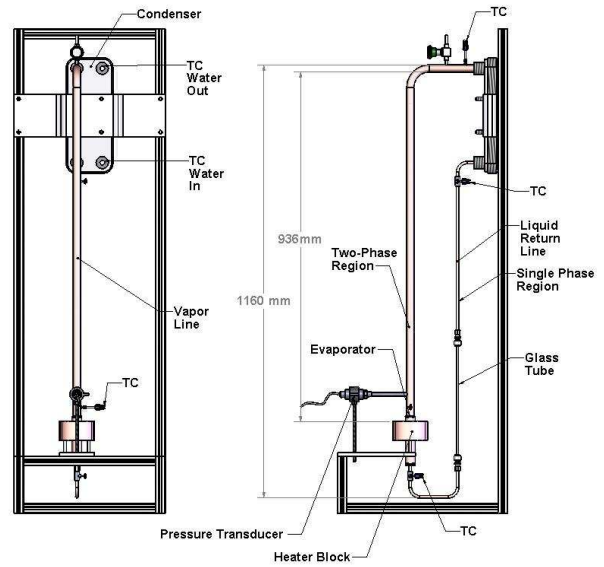


Figure 4. An overall schematic of the loop thermosyphon is shown.

The cylindrical heater block was fabricated from copper and included twenty (20) 6.35mm diameter cartridge heaters positioned circumferentially around the evaporator perimeter. The heater block design, shown in Figure 6, was stepped from 50.8mm in height to 12.7mm. The 12.7mm region was brazed to the evaporator wall and provided the heat input area of 10cm². A cross sectional view of the evaporator is also shown in Figure 6. A variable transformer was wired to supply power to the cartridge heaters. The evaporator also included a series

of eight holes, positioned in pairs at four radial locations around the evaporator for the purpose of conduction calorimetry. The thermal load applied to the heat input region was calculated at these four radial locations around the evaporator, by measuring the temperature difference across the thermocouples at these locations and knowing the geometry of the heater block and material thermal conductivity. The thermocouple locations were spaced so an accurate measurement of the heat fluxes, wall temperatures and heat transfer coefficients would be achieved. The uncertainty in the heat transfer coefficients measurements were $\pm 8\%$ at low heat fluxes and $\pm 3\%$ at higher heat fluxes.



Figure 5. Photographs of the annular wick (left) and biporous slab wick with vapor vents (right) are shown.

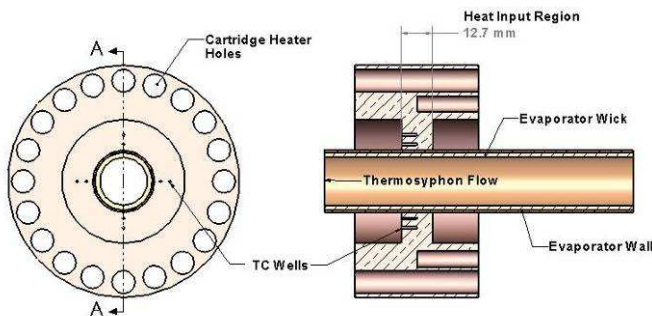


Figure 6. A detailed drawing of the evaporator design is shown.

A total of fourteen thermocouples, including the heater block thermocouples, were mounted with the prototype hardware to measure performance. Type K thermocouples were used in the heater block and Type T were used in the remaining loop structure. The vapor line exiting the evaporator included a thermocouple well within the vapor space and a pressure transducer port to provide an accurate measurement of the fluid pressure exiting the evaporator. A thermocouple well was also mounted within the vapor line vapor space at the entrance of the condenser, and within the liquid return line at the entrance to the evaporator. An energy balance over the condenser was measured using thermocouples mounted within the heat exchanger coolant inlet and exit lines and a measured flow rate. The entire assembly was insulated in a ceramic fiber blanket to minimize thermal losses. The thermocouples and pressure transducer were interfaced with a Keithley Model 2700 data acquisition computer system. The data acquisition

system is capable of taking 80 measurements at 22-bit accuracy every second. The data was monitored graphically in real time and recorded for future analyses.

TEST PROCEDURE

Tests were performed at two fluid inventories: 100cm^3 and 200cm^3 . The purpose of the lower fluid charge was to investigate the heat transfer coefficient and critical heat flux when the liquid was partially pulled to the heat input region by the capillary forces of the wick. The purpose of the larger fluid charge was to investigate the similar phenomena when the full liquid column was able to supply the maximum liquid flow rate. Power was applied to the cartridge heaters to achieve an initial power of several hundred watts and the thermal performance monitored. The saturated vapor temperature in the loop was set at 70°C . This temperature was selected because it would provide enough driving force to meet wall temperature requirements of 125°C , while also allowing the physical properties of the fluid (in particular the vapor density) to remain sufficient enough to result in low vapor velocity and low vapor friction losses to achieve a high critical heat flux. The coolant water flow rate was controlled to maintain the set point temperatures as power input was changed. The temperatures and pressures were monitored until steady state was achieved. During testing the energy balance was monitored by comparing the power transferred to the evaporator calculated via conduction calorimetry to the power removed through the condenser by sensible heating on the cooling water. Figure 7 shows the thermal circuit model at the heater block from the measured temperatures (T_{H1} and T_{H2}) to the fluid temperature T_{f0} . The wall temperature was calculated by extrapolating the two measured heater block temperatures to the surface of the tube wall. The heat transfer coefficient was calculated using this calculated wall temperature and the measured fluid temperature, T_{f0} , leaving the evaporator. The thermal resistance of the braze joint between the heater block and the evaporator body was calculated using a thickness of 0.051mm and properties of copper. These calculations were repeated for the four sets of thermocouples in the heater block, each positioned 90° from each other. These measurements were then averaged to determine the reported values. This process was continued for each evaporator design until a dry out condition was reached.

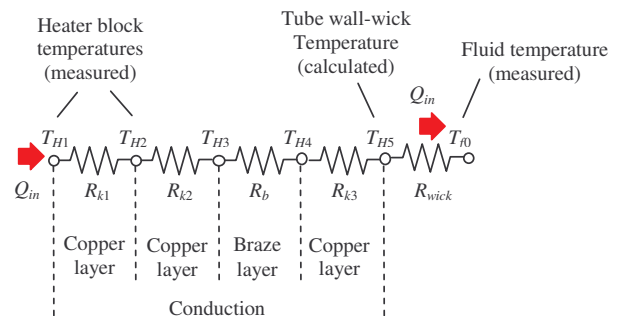


Figure 7. The thermal resistance network around the evaporator region is illustrated.

RESULTS AND DISCUSSION

Thermal performance tests were conducted on each of the three evaporator wick structures at 100cm³ and 200cm³ fluid charges. The data from the monoporous wick structure at 200cm³ fluid charge is shown in Figure 8 to illustrate the method in which critical heat flux was measured. Plotted is the wall to vapor ΔT ($T_{\text{wall}} - T_{\text{vapor}}$), the average wall temperature, the heat flux, the vapor temperature exiting the evaporator, and the average power input determined by conduction calorimetry. Dryout is shown to occur when the wall temperature shows a sharp discontinuity. The loop thermosyphon using the monoporous wick transferred a maximum of approximately 2,280W at 240W/cm², while maintaining an approximate 70°C-80°C bulk vapor temperature. The wall temperature increased from 129°C to 137°C when dryout occurred.

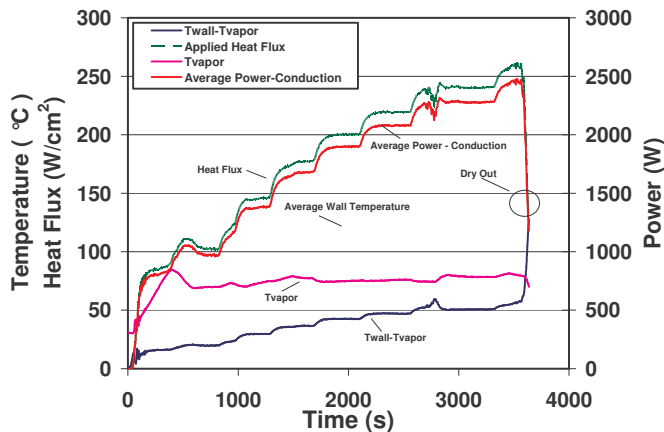


Figure 8. A plot of temperatures and power versus time as power is increased until critical heat flux is shown.

The heat transfer coefficient at each steady state point up to dryout is plotted as a function of heat flux for each wick design and fluid charge. The results are presented in Figure 9. The solid lines and dashed lines indicate the data at 100cm³ and 200cm³ fluid charges, respectively. At 100cm³ each of the evaporator wick designs reached an approximate critical heat flux (CHF) as follows: monoporous at 186W/cm², biporous at 88W/cm², and biporous with integral vapor vents at 154W/cm². The heat transfer coefficients were between approximately 3.3 W/cm²°C and 4.98W/cm²°C. The critical heat flux extended for each design at 200cm³ fluid charge. The monoporous CHF increased to 260W/cm², the biporous extended to 463W/cm², and biporous with integral vapor vents extended to 368W/cm². The heat transfer coefficient significantly decreased at the increased CHF for the biporous designs. The monoporous design decreased slightly from approximately 5.0W/cm²°C to 4.5W/cm²°C, while the biporous and the biporous design with integral vapor vents dropped significantly from approximately 4.3W/cm²°C to 1.15W/cm²°C.

The CHF extension with the additional fluid charge was expected as the increase in flow rate of the liquid more amply

supplied liquid to the wick. The heat transfer coefficient remained constant at the higher fluid charge as the fluid dynamics within the wick are not appreciably altered by the increase in convection on the outside of the wick. At these high heat fluxes it was also expected that the mode of heat transfer in this flow boiling case would be dominated by the pool boiling contribution rather than the forced convective contribution to the total heat transfer coefficient [5].

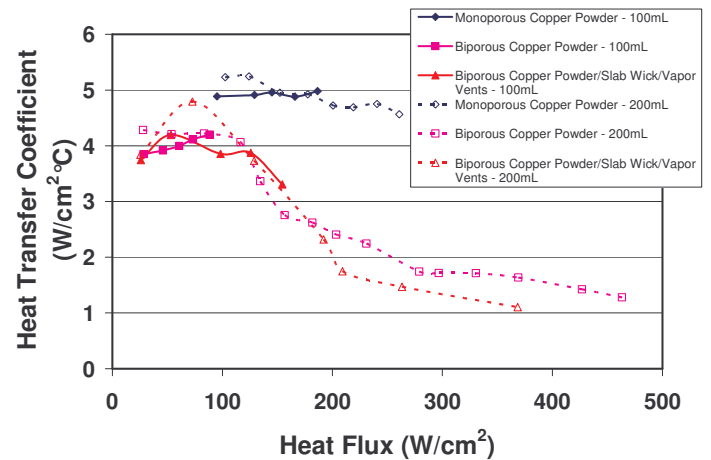


Figure 9. A plot of the measured heat transfer coefficients versus measured heat flux (until critical heat flux) is shown for the three evaporators at two flow rates.

For the monoporous wick design, the heat transfer coefficient was independent of heat flux compared to the steady decrease in heat transfer coefficient compared to both biporous wick designs. This is believed to be caused by a decrease of liquid in the biporous wick as the higher flow rate of vapor leaving the inner wick occupies a larger volume of liquid in the wick as heat flux increases. The biporous wick structure is made of clusters of small diameter particles, where liquid wicks using the high available capillary pressure within the cluster, but flows easier in the space between the clusters. At low heat fluxes, the fluid can still flow in the spaced between the clusters and fully wet the wall of the heat input surface, maintaining heat transfer coefficient closer to monoporous designs.

In this flow boiling configuration with a large heat input region, liquid is supplied axially through the wick as well as flow radially from the liquid flow through the evaporator. At higher heat fluxes the available capillary pumping pressure of the wick to adequately supply fluid axially to the center of the heat input region may be limited. The liquid flowing through the center core of the evaporator wetting the outer wick surface dominates the liquid contribution to the heat input area. The liquid is transported through the porous structure normal to the surface through the clusters as the permeable channels are occupied by vapor at high heat fluxes. The low flow resistance path for vapor escape causes an increase in CHF associated

with the biporous wicks. However, the occupation of vapor rather than liquid in these channels also starves the wall of liquid, lowering the heat transfer coefficient. The biporous wick with the integral vapor vents did not perform as well as the annular biporous wick. In this configuration, the flow boiling is restricted due to the slab wick occupying the evaporator vapor core. Future designs will modify the slab wick to include a liquid and vapor flow path.

CONCLUSIONS

A loop thermosyphon was constructed in anticipation of reaching a heat flux goal of $1\text{kW}/\text{cm}^2$ over a 10cm^2 area. The device was tested using three wick designs at two fluid charges. The larger fluid charge performed better with respect to critical heat flux for all cases as liquid was more amply supplied to the wick. The biporous wick performed better with respect to critical heat flux capability compared to the monoporous design. The biporous wick did not provide heat transfer coefficients as high as the monoporous wick at high heat fluxes as liquid was not able to wet the wall well enough due to vapor occupying the large voids within the powder. At 200cm^3 fluid charge the maximum power carried by the loop thermosyphon and the associated heat flux for each of the wick structures to cool the 10cm^2 area prior to dryout is as follows: monoporous, $2,280\text{W}/240\text{Wcm}^2$, biporous, $4,390\text{W}/465\text{Wcm}^2$, biporous with vapor vents, $3,488\text{W}/367\text{Wcm}^2$.

ACKNOWLEDGMENTS

This work was performed for the United States Navy, Office of naval Research under UCLA Contract Number N00014-04-1-0280. The technical monitor was Dr. Mark Spector. The authors would like to acknowledge Michael Ames, Michael Devine, and Chris Stover for assistance in the design, assembly and testing of the prototype loop thermosyphon.

REFERENCES

- [1] Zerby, M., 2002, "Next Generation Navy Thermal Management", NSWCCD-82-TR-2002/12, March 2002.
- [2] Semenic, T., Lin, Y., Catton, I., 2005a, "Use of Liquid Film Evaporation in Biporous Media to Achieve High Heat Flux over Large Areas," *Proceedings of ASME Summer Heat Transfer Conference*, Paper Number HT2005-72238, July 17-22, 2005.
- [3] Semenic, T., Catton, I., 2005b, "Heat Removal and Thermophysical Properties of Biporous Evaporators," *Proceedings of 2006 ASME International Mechanical Engineering Congress and Exposition*, Paper Number IMEC2006-15928, November 5-10, 2006.
- [4] Lin, Y., Semenic, T., Catton, I., 2005, "Thermophysical Properties of Monoporous Sintered Copper, *Proceedings of ASME Summer Heat Transfer Conference*, Paper Number HT2005-72239, July 17-22, 2005.

[5] Collier, J.G. and Thome, J.R., 1996, "*Convective Boiling and Condensation*", 3rd Edition, Oxford University Press, Oxford (paperback edition).

[6] Wallis, G.B., 1969, "*One Dimensional Two-Phase Flow*", McGraw-Hill, New York.

[7] Lockhart, R.W. and Martinelli, R.C., 1949, "Proposed Correlation of Data for Isothermal Two-Phase Two-Component Flow in Pipes", *Chem. Eng. Prog.*, 45, 39.

[8] Martinelli, R.C. and Nelson, D.B., 1948, "Prediction of Pressure Drop During Forced Circulation of Boiling Water", *Trans, ASME*, 70, 695.